ACS Infectious Diseases

pubs.acs.org/journal/aidcbc

Article

Inhibition of Human Coronaviruses by Antimalarial Peroxides

Ayan Kumar Ghosh,[#] Halli Miller,[#] Konstance Knox, Madhuchhanda Kundu, Kelly J. Henrickson, and Ravit Arav-Boger*

Cite This: https://doi.org/10.1021/acsinfecdis.1c00053

Read Online

ACCESS | Metrics & More | Article Recommendations | Supporting Information

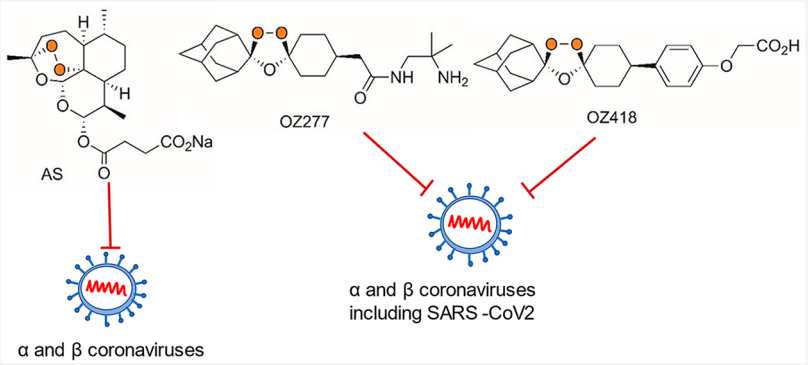

ABSTRACT: As the toll of the severe acute respiratory syndrome coronavirus 2 (SARS-CoV-2) pandemic continues, efforts are ongoing to identify new agents and repurpose safe drugs for its treatment. Antimalarial peroxides have reported antiviral and anticancer activities. Here, we evaluated the *in vitro* activities of artesunate (AS) and two ozonides (OZ418 and OZ277) against human α-coronavirus NL63 and β-coronaviruses OC43 and SARS-CoV-2 in several cell lines. OZ418 had the best selectivity index (SI) in NL63-infected Vero cells and MK2 cells. The overall SI of the tested compounds was cell-type dependent. In OC43-infected human foreskin fibroblasts, AS had the best cell-associated SI, $\geq$17 μM, while the SI of OZ418 and OZ277 was $\geq$12 μM and $\geq$7 μM, respectively. AS did not inhibit SARS-CoV-2 in either Vero or Calu-3 cells. A comparison of OZ418 and OZ277 activity in SARS-CoV2-infected Calu-3 cells revealed similar EC_{50} (5.3 μM and 11.6 μM, respectively), higher than the EC_{50} of remdesivir (1.0 $\pm$ 0.1 μM), but the SI of OZ418 was higher than OZ277. A third ozonide, OZ439, inhibited SARS-CoV-2 efficiently in Vero cells, but compared to OZ418 in Calu-3 cells, it showed higher toxicity. Improved inhibition of SARS-CoV-2 was observed when OZ418 was used together with remdesivir. Although the EC_{50} of ozonides might be clinically achieved in plasma after intravenous administration, sustained virus suppression in tissues will require further considerations, including drug combination. Our work supports the potential repurposing of ozonides and calls for future *in vivo* models.

KEYWORDS: *coronaviruses, SARS-CoV-2, artemisinins, ozonides, remdesivir, combination*

Coronavirus (CoV) disease 19 (COVID-19), the respiratory illness caused by Severe Acute Respiratory Syndrome CoV 2 (SARS-CoV-2), has had severe global effects on human health.[1] Continuous waves of disease are alarming, requiring development of preventive and therapeutic measures that are safe and cost-effective. Researchers across the world are devoted to identifying vaccines and safe therapeutics for SARS-CoV-2.[2,3] Repurposing of remdesivir (GS-5734), an inhibitor of the viral RNA-dependent RNA polymerase, has shown promising results in clinical trials, although debate continues regarding its efficacy.

The α- and β-CoVs infect humans, and four CoVs are prevalent in the population: α-CoV 229E and NL63 and β-CoV OC43 and HKU1.[4] Although the β-CoVs OC43, MERS-CoV, SARS-CoV, and SARS-CoV-2 show a high degree of conservation of essential functional domains, their response to antiviral agents has shown some differences. For example, the combination of lopinavir and ritonavir had benefits in patients infected with SARS-CoV and MERS-CoV,[5] but no benefit was observed in adults infected with SARS-CoV-2.[6] Several drugs studied until now for COVID-19 have been repurposed from other indications, to allow faster track therapeutics. These include the antimalarials hydroxychloroquine (with or without azithromycin), chloroquine, and remdesivir, immune modulating agents,[7−9] and virus-neutralizing monoclonal antibodies.[10]

Special Issue: In Celebration of Jonathan Vennerstrom: A Pioneer in Neglected Tropical Diseases

Received: January 29, 2021

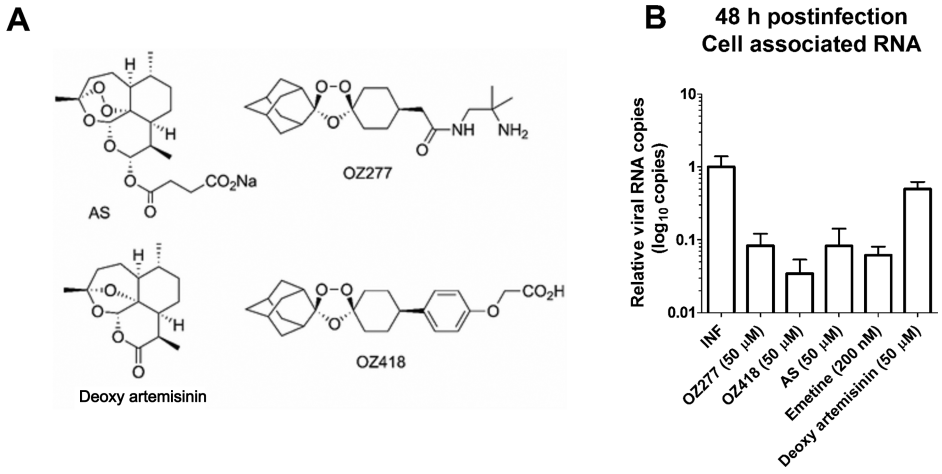

Figure 1. Anti-NL63 activity of AS, deoxy artemisinin, and ozonides. (A) Chemical structures of sodium AS, deoxy artemisinin, OZ277, and OZ418. (B) Vero cells were infected with CoV NL63 and treated for 48 h with OZ277, OZ418, AS, deoxy artemisinin, or emetine at the indicated concentrations. Cell associated viral RNA levels were quantified by qRT-PCR and normalized to the RNA level in nontreated, infected Vero cells, in addition to internal normalization of each sample to cellular GAPDH RNA. Emetine (200 nM) was used as a positive control for anti-CoV activity. The data represent mean values (±SD) of triplicate determinations from two independent experiments.

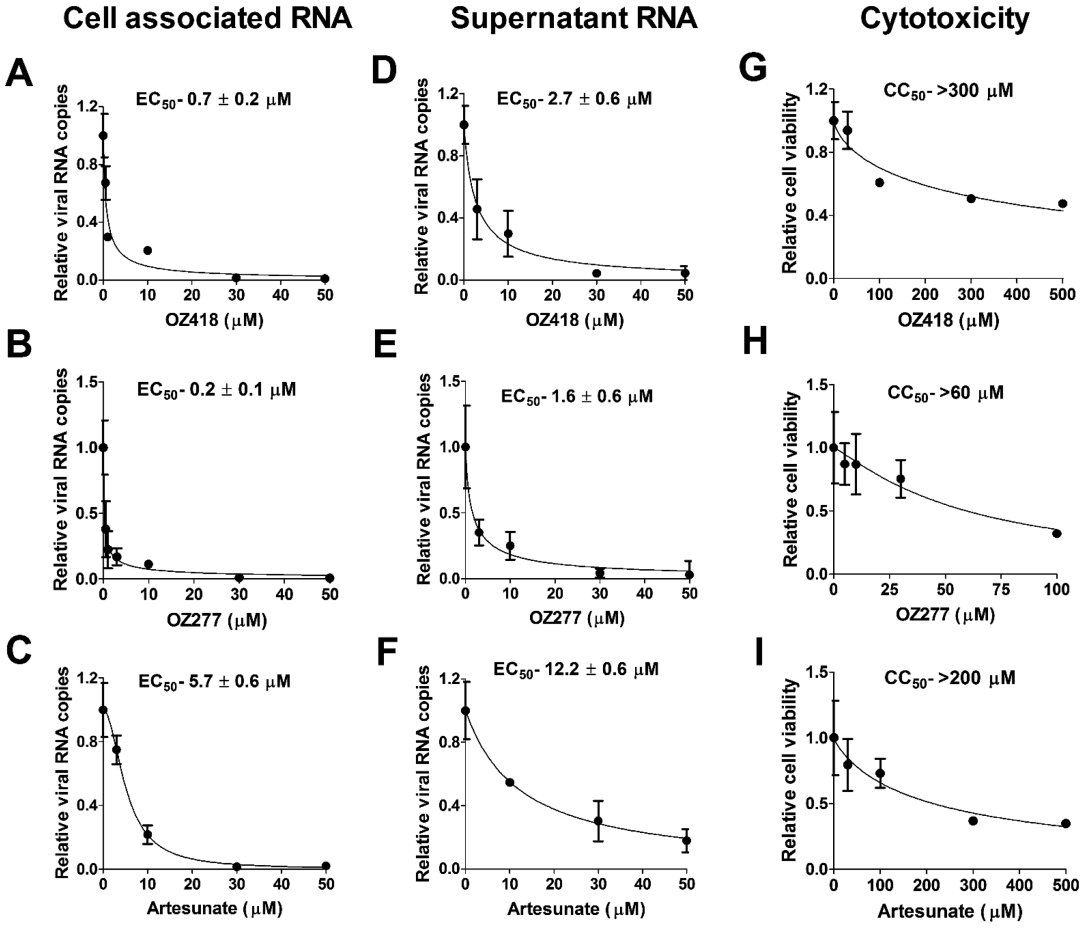

Figure 2. EC_{50} and CC_{50} of OZ and AS against NL63-infected Vero cells. (**A**–**C**) Dose–response curves and EC_{50} values of OZ418, OZ277, and AS. Vero cells were infected with NL63 and treated for 72 h with the indicated concentrations of the drugs. Culture supernatants were harvested, and cells were lysed for RNA isolation and qRT-PCR as described in Figure 1B. (**D**–**F**) Dose–response curves and EC_{50} values of OZ418, OZ277, and AS were generated from the viral RNA isolated from culture supernatants. Culture supernatants were harvested at 72 hpi, and viral RNA was isolated. Relative viral RNA was calculated by dividing the calculated copy number of viral RNA obtained following treatment of each drug by the viral RNA calculated copy number of the untreated, infected culture supernatant. (**G**–**I**) The MTT assay was performed in noninfected Vero cells using different concentrations of drugs. Vero cells were treated with DMSO (vehicle control) or different concentrations of OZ418, OZ277, or AS for 72 h. The EC_{50} and CC_{50} values represent mean values (±SD) of triplicate determinations from two independent experiments.

https://doi.org/10.1021/acsinfecdis.1c00053
ACS Infect. Dis. XXXX, XXX, XXX–XXX

Table 1. EC_{50}, CC_{50}, and SI of OZ and AS against CoV

cell/virus		compound			
		OZ418	OZ277	artesunate	OZ439
Vero/NL63	EC50 (μM)[a]	0.7 ± 0.2	0.2 ± 0.1	5.7 ± 0.6	
	EC50 (μM)[b]	2.7 ± 0.6	1.6 ± 0.6	12.2 ± 0.6	
	CC50 (μM)	>300	>60	>200	
	SI[a]	**≥428**	**≥300**	**≥35**	
	SI[b]	**≥111**	**≥37**	**≥16**	
MK2/NL63	EC50 (μM)[a]	0.5 ± 1.3	0.5 ± 0.04	2.4 ± 1.4	
	EC50 (μM)[b]	1.0 ± 0.3	1.6 ± 0.3	8.5 ± 1.5	
	CC50 (μM)	>300	>90	>400	
	SI[a]	**≥600**	**≥180**	**≥167**	
	SI[b]	**≥300**	**≥56**	**≥47**	
HFF/OC43	EC50 (μM)[a]	9.7 ± 1.8	4.3 ± 0.1	4.0 ± 1.4	
	EC50 (μM)[b]	9.4 ± 1.9	4.2 ± 1.7	11.5 ± 2.6	
	CC50 (μM)	>120	>30	>70	
	SI[a]	**≥12**	**≥7**	**≥17**	
	SI[b]	**≥13**	**≥7**	**≥6**	
Vero E6/SARS CoV-2	EC50 (μM)[a]	23 ± 1.8	8.5 ± 0.2	NA	
	EC50 (μM)[b]	14.2 ± 7.1			3.0 ± 0.1
	CC50 (μM)	>300	>60		>500
	SI[a]	**≥13**	**≥7**		
	SI[b]	**≥21**			100 ± 3.4
Calu-3/SARS-CoV-2	EC50 (μM)[b]	5.3 ± 3.7	11.6 ± 2	NA	11.5 ± 2.5
	CC50 (μM)	>300	>70		>60
	SI[b]	**≥57**	**≥6**		**≥5**

[a]Cell associated viral RNA. [b]Supernatant viral RNA, NA − no activity. The SI is provided as ≥ rather than an exact value, since the measured CC_{50} did not approach 0.

The antimalarial agents, artemisinins, as well as their fully synthetic versions (ozonides) have shown activity against several DNA and RNA viruses.[11] Although ozonides (1,2,4-trioxolanes) have a similar mode of action to artemisinins against the malaria parasites, they have shown an extended half-life in animal models,[12,13] providing therapeutic advantage not only for the treatment of malaria but also for repurposing to other indications. OZ277 (arterolane) was registered in India in 2011 for antimalarial therapy in combination with piperaquine.[14] The next-generation ozonide, OZ439 (artefenomel), exhibits an increased pharmacokinetic half-life and good safety profile and is being tested in phase IIb clinical trials.[12,15,16] OZ418 has reported antischistosomal activity.[13] The detailed *in vitro* activity of artesunate and ozonides against human CoV is reported here.

RESULTS

Inhibition of α-CoV with Artesunate and Ozonides. To screen for ozonides' activity against α-CoV, Vero cells were infected with NL63 at a multiplicity of infection (MOI) of 0.001 PFU/cell. Immediately following infection, cells were treated with artesunate (AS), deoxy artemisinin−which lacks the critical peroxide pharmacophore, ozonide (OZ) 418 or OZ277 at 50 μM (Figure 1A, chemical structure), or emetine at 200 nM for 48 h (Figure 1B). Emetine reportedly inhibits α- and β-CoV *in vitro*.[17] All compounds reduced viral RNA in the cellular compartment by 90−95% compared to untreated infected samples (Figure 1B). Deoxy artemisinin reduced viral RNA only by ∼50%, suggesting the oxygen bridge contributes to NL63 inhibition.

To further examine the activity of OZ and AS on NL63 RNA at 72 h postinfection (hpi), dose−response curves were generated using qRT-PCR. Cellular toxicity was tested by the MTT assay in noninfected cells at the same time point (Figure 2, Table 1). The following concentrations were used: 500 nM−50 μM for OZ418 and OZ277 and 3−50 μM for AS. NL63 RNA was reduced by OZ418 and OZ277 at submicromolar concentrations and showed better inhibition than AS in the cellular compartment (Figure 2A−C, Table 1). The EC_{50} of OZ was also lower than AS in the supernatants (Figure 2D,E, Table 1), 4.5−7.8-fold greater inhibition than AS (Figure 2F, Table 1). The 50% cell viability (CC_{50}) of OZ418 was higher than OZ277 (Figure 2G−I, Table 1). The cell associated EC_{50} of the compounds was used to determine the selectivity index (SI) (Table 1). In Vero cells, OZ418 had the most favorable SI (Table 1).

We next tested the inhibition of NL63 RNA by ozonides in another epithelial cell line, MK2. A similar inhibitory pattern by OZ418, OZ277, and AS was observed (Figure 3, Table 1). In the cellular compartment, OZ418 and OZ277 showed similar inhibition of viral RNA (Figure 3A,B, Table 1). Inhibition of NL63 RNA by AS in the cellular compartment was 2.4-fold greater in MK2 cells than in Vero cells (Figures 2C and 3C, Table 1) but again reduced compared to OZ. OZ418 showed a 2.7-fold reduction in EC_{50} by released (supernatant) viral RNA in MK2 cells compared to Vero cells (Figures 2D and 3D, Table 1). The EC_{50} of OZ277 measured in MK2 supernatants was similar to the EC_{50} observed in Vero cells (Figures 2E and 3E, Table 1). In MK2 cells, the EC_{50} of AS for released viral RNA was 1.4-fold lower than the observed EC_{50} in Vero cells (Figures 2F and 3F, Table 1). Similar to the SI in Vero cells, OZ418 had the highest SI among the compounds tested (Table 1).

Inhibition of β-CoV OC43 by AS and OZ. To test whether OZ had activity against both α- and β-CoV, compounds were tested against OC43-infected human foreskin

https://doi.org/10.1021/acsinfecdis.1c00053
ACS Infect. Dis. XXXX, XXX, XXX−XXX

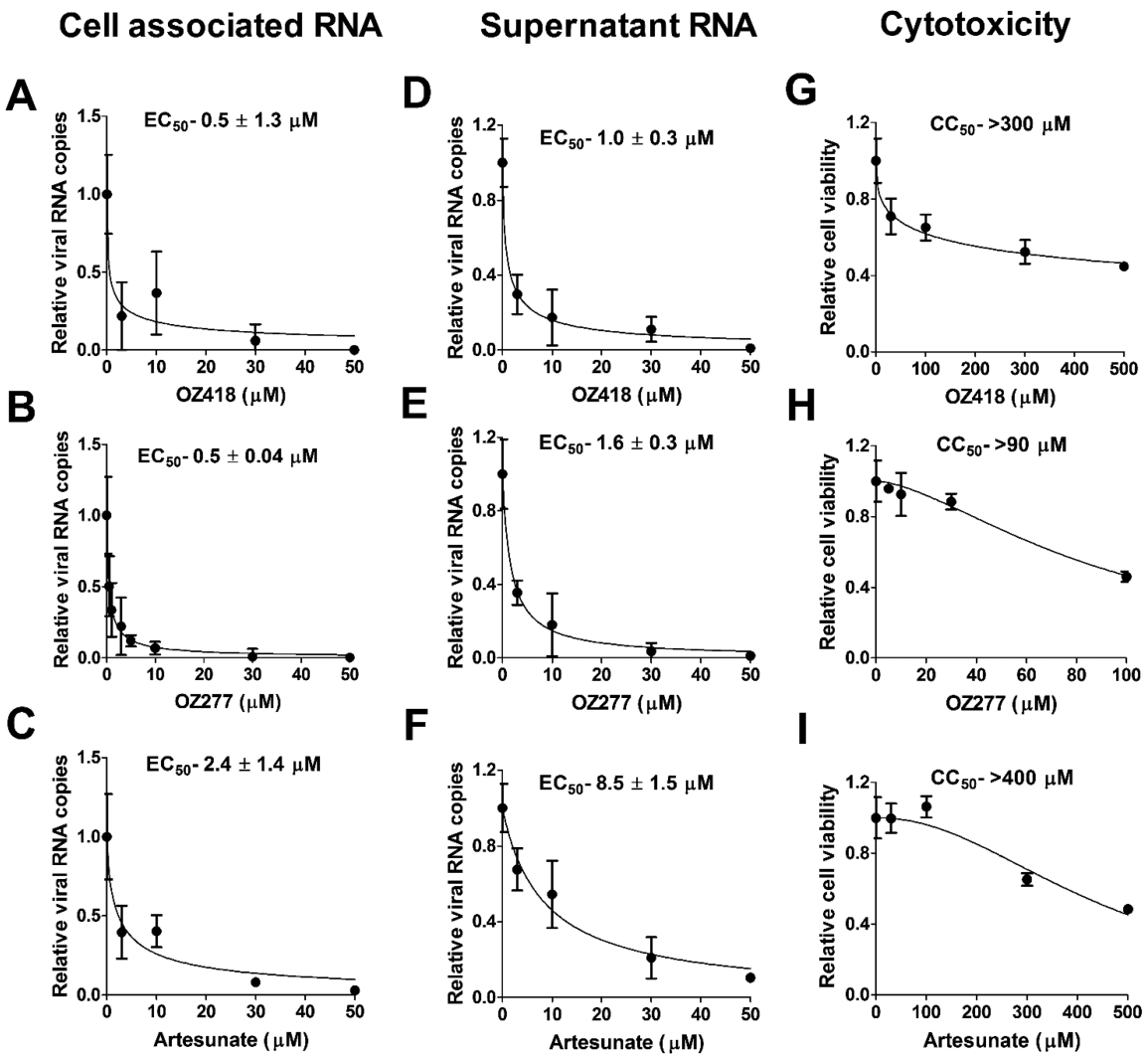

Figure 3. EC_{50} and CC_{50} of OZ and AS against NL63-infected MK2 cells. (**A**–**C**) Dose–response curves and EC_{50} values of OZ418, OZ277, and AS. MK2 cells were infected with NL63 and treated with the indicated concentrations of drugs for 72 h. Cells were lysed for RNA isolation and qRT-PCR. (**D**–**F**) Dose–response curves and EC_{50} values of OZ418, OZ277, and AS were generated from viral RNA isolated from culture supernatants of infected MK2 cells. (**G**–**I**) The MTT assay was performed in noninfected MK2 cells using different concentrations of drugs. Quantitative data represent mean values (±SD) of triplicate determinations from two independent experiments.

fibroblasts (HFF), MOI = 0.01 (Figure 4). Dose–response experiments were performed at concentrations of 500 nM–50 μM for OZ418 and OZ277 and 3–50 μM for AS. All three compounds effectively reduced OC43 RNA in the cellular compartment and in the supernatant (Figure 4, Table 1). The EC_{50} of OZ418 and OZ277 in the cellular compartment and the supernatant was comparable. The EC_{50} of AS in the cellular compartment (Figure 4C, Table 1) was approximately 2.9-fold lower than in the supernatant (Figure 4F, Table 1). Based on the calculated CC_{50} and EC_{50}, in OC43-infected HFFs, AS had the highest cell associated SI (Table 1).

A Western blot was performed on infected cellular lysates harvested at 72 hpi. The expression of the OC43 antigen was reduced by OZ418 (30 μM), OZ277 (15 μM), and AS (30 μM) (Figure 4G), although the effect of AS was lower compared to OZ418 and OZ277. Emetine (200 nM), used as a positive control, showed complete inhibition of the CoV-OC43 antigen.

Inhibition of SARS-CoV-2 with OZ. The activity of OZ and AS was tested in Vero E6 by the cytopathic effect at 72 hpi (CPE, Figure 5A,B) and in Calu-3 by qRT-PCR at 48 hpi (Figure 5C,D). Remdesivir was used as a positive control in Vero cells (Figure 5C). SARS-CoV-2 suppression by OZ418 and OZ277 was not significantly different, but OZ277 showed higher toxicity in Calu-3 cells. AS at 30 μM did not inhibit SARS-CoV-2 in either cell type. In addition, AS had no activity against SARS-CoV-2 irrespective of the serum concentration in infected Vero cells (2% or 4%). No effect of AS was observed on SARS-CoV-2 RNA at 24 h in infected Calu-3 cells. Additional testing was performed with OZ439 (artefenomel), which is currently in clinical trials for malaria (Figure S1).[12] In Vero E6 cells, OZ418 and OZ439 (30 μM) decreased the viral RNA load by 4 and 1.5 logs, respectively (Figure S1A). Based on the relative biomass, OZ439 had improved activity compared to OZ418 (Figure S1B,C). In Calu-3 cells, OZ418 and OZ439 reduced the viral RNA virus by 2 and 1 logs, respectively (Figure S1D); however, the biomass analysis revealed higher toxicity of OZ439 in these cells (Figure S1E,F). OZ418 was superior to OZ439 in the overall antiviral activity and preservation of the monolayer in Calu-3 cells.

Combination of OZ and Remdesivir (RDV) against β-CoV OC43 and SARS-CoV-2. To determine the effect of

https://doi.org/10.1021/acsinfecdis.1c00053
ACS Infect. Dis. XXXX, XXX, XXX–XXX

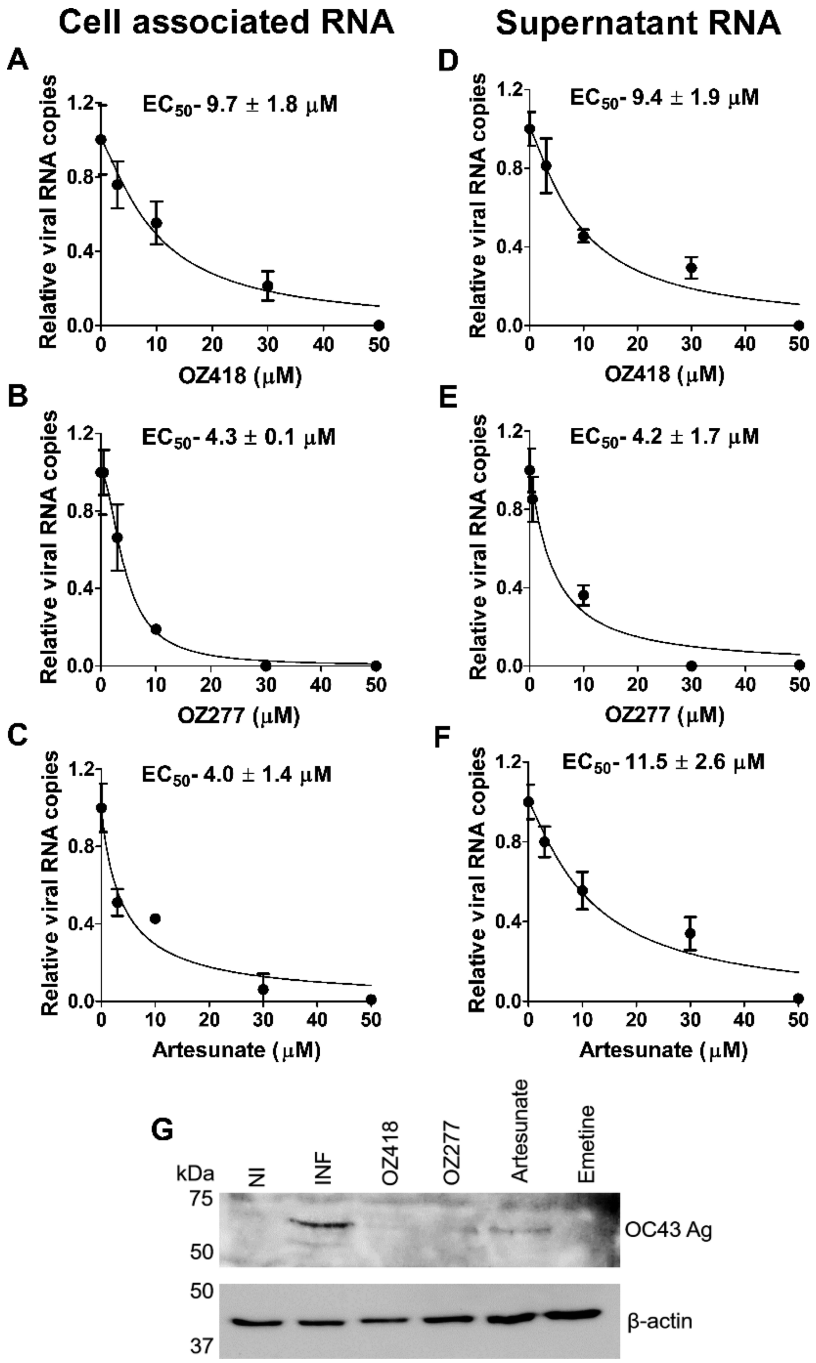

Figure 4. EC_{50} of OZ and AS against OC43-infected HFFs. (**A**−**C**) Dose−response curves and EC_{50} values of OZ418, OZ277, and AS. HFF cells were infected with OC43, treated with the indicated concentrations of the drugs, and incubated for 72 h. Culture supernatants were harvested, and cells were lysed for RNA isolation and qRT-PCR. (**D**−**F**) Dose−response curves and EC_{50} values of OZ418, OZ277, and AS were generated from viral RNA isolated from the culture supernatant of infected HFFs. Quantitative data represent mean values (±SD) of triplicate determinations from two independent experiments. (**G**) Inhibition of OC43 based on Western blot analysis. Infected cells (MOI = 1) were harvested at 72 hpi, and Western blot analysis was performed as described in the Methods section. NI − noninfected control and INF − infected controls.

OZ418 in drug combination, we tested the effect of remdesivir and OZ alone and in combination against OC43. RDV alone had strong inhibition of the OC43 level at low nM concentration and improved the activity of OZ418 at both 5 μM and 10 μM (Figure 6A).

The combination of OZ418 and RDV was next tested in SARS-CoV-2-infected Calu-3 and Vero E6 cells (Figure 6 B,C). In both cells, the addition of RDV to OZ418 (15 μM) supported further protection of the biomass, suggesting improved activity (Figure S2).

DISCUSSION

The rationale for testing the anti-CoV activity of artemisinins and ozonides is based on recent findings from our laboratory that artemisinins target vimentin for human cytomegalovirus inhibition[18] and previous reports of the critical role of surface vimentin for cell entry of SARS-CoV.[19] Vimentin was present

https://doi.org/10.1021/acsinfecdis.1c00053
ACS Infect. Dis. XXXX, XXX, XXX−XXX

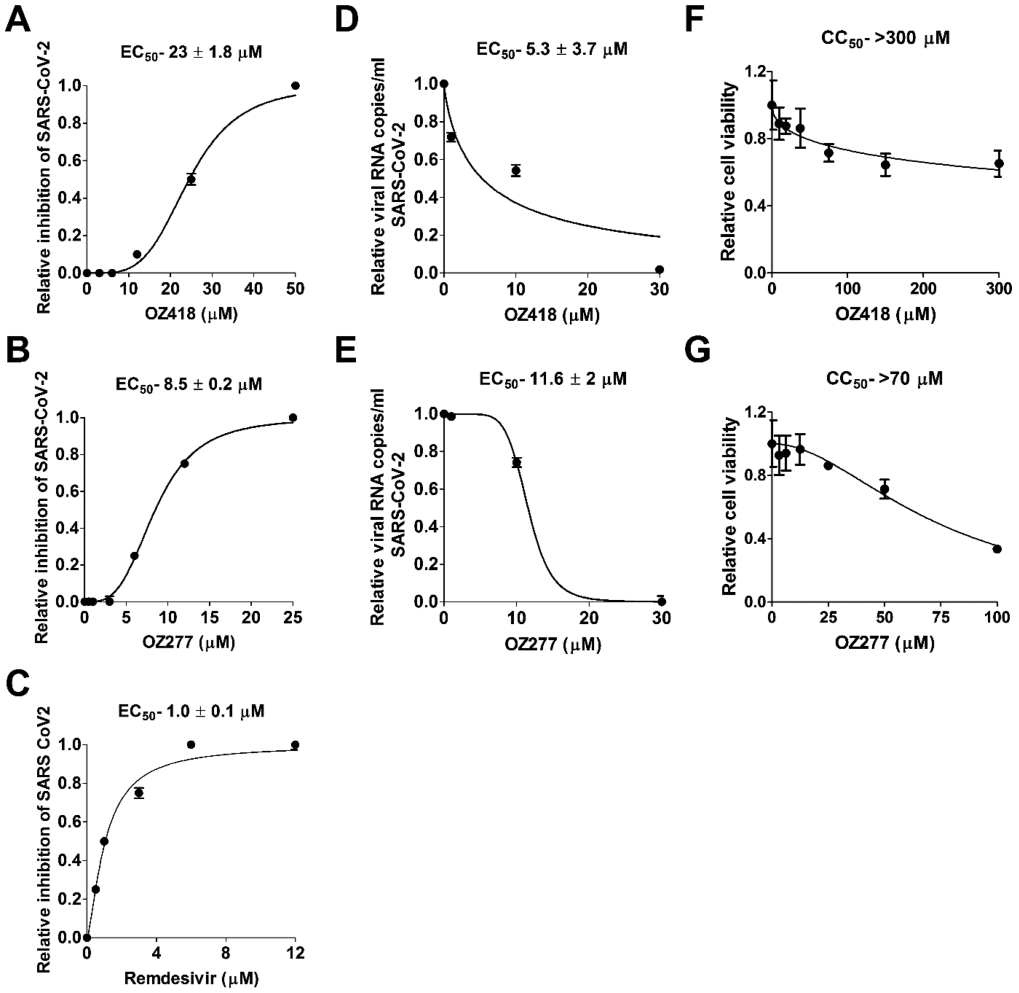

Figure 5. Inhibition of SARS-CoV-2 with OZ in Vero and Calu-3 cells. (**A**−**C**) Dose response curves and EC_{50} values of OZ418, OZ277, and remdesivir, respectively. Vero E6 cells were infected with SARS-CoV-2 (MOI = 0.05) and treated with the indicated concentrations of drugs for 72 h. The cells were then stained by crystal violet, and the cytopathic effect was analyzed by microscopy in each condition on a scale of 0−1 where 0 denotes complete CPE and 1 denotes 100% inhibition of the virus. The plots indicate relative inhibition compared to infected controls. (**D, E**) Dose response curves and EC_{50} values of OZ418 and OZ277. Calu-3 cells were infected with SARS-CoV2 and tested with the indicated concentrations of drugs for 48 h, supernatants were harvested, and qRT-PCR was performed. The plots indicate viral RNA copies compared to infected controls. (**F, G**) CC_{50} values calculated based on the MTT assay performed after 48 h of treatment with the indicated concentrations of OZ418 and OZ277 in Calu-3 cells. Data represent mean values (±SD) of triplicate determinations from two independent experiments.

in the complex of SARS-CoV spike protein angiotensin-converting enzyme 2 (ACE2) and was directly bound to the SARS-CoV spike protein, suggesting it serves as a coreceptor with ACE2 during a SARS-CoV infection.

Repurposing of the antimalarial agents, artemisinins, for treatment of viral infections attracted interest, fueled by clinical experience, safety data from malaria therapy, and cost.[20,21] Several artemisinin monomers (AS and artemether) are approved for malaria therapy.[20] AS has a good safety profile and tolerability in adults and children.[21] Artemether-lumefantrine (Coartem) is FDA-approved and commonly used in children. Others and we reported that artemisinin-derived monomers inhibit human cytomegalovirus (CMV) *in vitro* at μM concentrations.[22−24] The endoperoxide bridge is essential for their antimalarial and antiviral activity[25,26] and has stimulated the development of fully synthetic endoperoxides including the trioxolane OZ277, which has been approved for malaria therapy as a fixed dose combination with piperaquine.[14] Additional modifications of the trioxolane structure may influence drug binding, half-life, and other therapeutic properties.

Artemisinins were reported to inhibit RNA viruses such as HCV and HIV,[11] although these studies have been limited. A dose-dependent effect against HCV *in vitro* and synergistic activity with hemin were reported.[27] AS reportedly showed modest activity against HIV-1[22] but was not active against influenza viruses.[28] Recently, AS was reported to reduce SARS-CoV-2 RNA in Vero E6 infected with the SARS-CoV-2 strain nCoV-2019BetaCoV/Wuhan/WIV04/2019.[29] However, other clinically relevant artemisinins (artemether, artemisinin, and artemisone) had an EC_{50} of 50 μM or higher. In addition, in that study, the MOI used was 0.01, and RT-PCR was performed at 24 hpi, while we used a higher viral input (MOI = 0.05), performed RT-PCR at 48 hpi, and assessed cellular destruction at 72 hpi.

Although artemisinin monomers inhibit human cytomegalovirus, a DNA herpes virus, the short half-life of AS and artemether may prohibit their use as antiviral agents. The serum concentration or area under the concentration time

https://doi.org/10.1021/acsinfecdis.1c00053
ACS Infect. Dis. XXXX, XXX, XXX−XXX

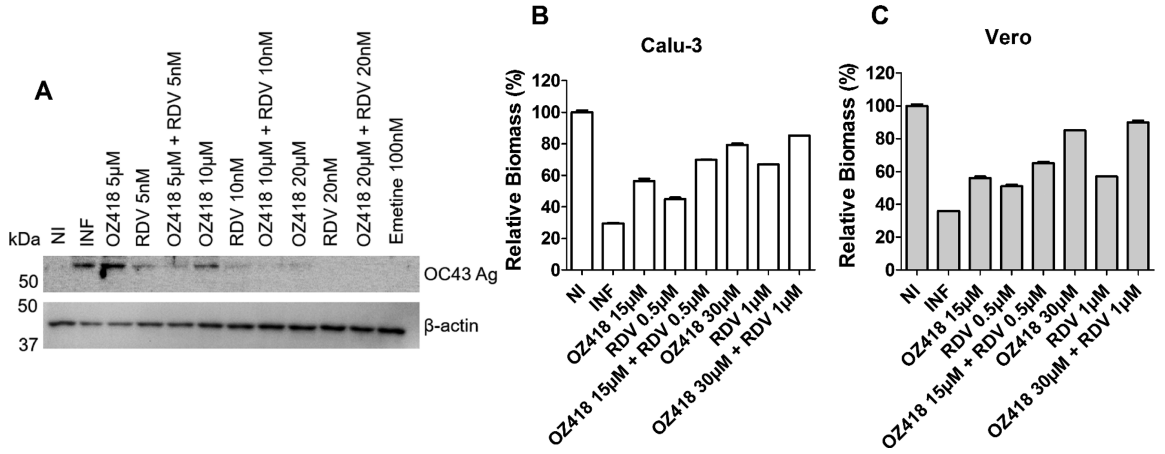

Figure 6. OZ418 and remdesivir (RDV) combination show improved virus suppression. (**A**) Western blot analysis of the effect of different concentrations of OZ418 and RDV and their respective combinations in OC43-infected HFF cells (MOI = 1). Emetine was used as a positive control, and β-actin was probed for an internal control. The Western blot image is representative of three independent experiments. (**B, C**) Monolayers of Calu-3 and Vero cells were infected with SARS-CoV-2 and treated with the indicated concentrations of OZ418 and RDV and their respective combinations for 72 h. Cells were thereafter stained with crystal violet, washed, and dissolved in 10% acetic acid. The solutions were then analyzed for absorbance at 595 nm. The plots are representative of the relative biomass, where 100% biomass indicates noninfected control cells, and 0% biomass indicates a complete cytopathic effect due to viral infection. The biomass assay represents mean (±SD) of duplicate (controls) or triplicate (combinations) determinations.

curve (AUC) achieved with the current dosing regimen of AS is unlikely to fully inhibit human CMV replication, and higher, frequent doses may result in side effects. Considering the half-life parameter for sustained virus suppression, we tested the anti-CMV activity of OZ, fully synthesized artemisinin-like monomers.[13] The *in vitro* activity of OZ against human CMV was similar to AS, but the *in vivo* activity in a mouse CMV model was significantly improved compared to AS.[30]

Our data reveal that the EC_{50} of OZ418, OZ277, and AS are stable and specific for the cell lines tested; it was higher in HFFs compared to the monkey epithelial cells. HFFs are used here for the first time for infection with CoV OC43. We note that OC43 does not bind to the ACE2 receptor; hence, vimentin may interact with additional cellular receptors to facilitate virus entry or intracellular processing.[31,32] The variability in the antiviral activity of artemisinins/ozonides in the different cell lines is consistent with the reported activity of artemisinins in different cancer cell lines[33] and suggests that the molecular target influences drug activity. It may also suggest differential usage of cellular receptors and coreceptors by NL63, OC43, and SARS-CoV-2 in the different cell types treated with OZ or artemisinins. A recent study showed differences in epithelial-mesenchymal transition (EMT), a process controlled by vimentin, between different origins of epithelial cells: alveolar (A549), bronchial (Calu-3), and colonic (Caco-2). When challenged with transforming growth factor-β1 (TGF-β1) or other pro-inflammatory cytokines, A549 cells underwent EMT, evidenced by a spindlelike morphology, increased vimentin, and downregulation of E-cadherin, an epithelial marker. In contrast, Calu-3 and Caco-2 cells failed to show morphological changes or alterations in marker expression associated with EMT.[34] These data suggest the effect of AS may depend on vimentin availability for binding, while OZ either have better affinity for vimentin or target additional cellular proteins. Although vimentin has been suggested as a target for treatment of SARS-CoV-2, better understanding of the effects of virus infection and antiviral agents on vimentin stability, post-translational modification, and protein interaction is required.[35] In the case of CMV, infection disassembled vimentin, and artemisinins stabilized vimentin early after infection.[18] Future studies are needed to better understand the biological effects of CoV on vimentin and the timing and effects of artemisinins/ozonides on vimentin during infection.

The observed differences in antiviral activity may be cell-based and/or reflect virus susceptibility.[36] Remdesivir was first tested by RT-PCR in Vero E6 and was active against SARS-CoV-2, with an EC_{50} of ∼0.77 μM. A more detailed comparison of its antiviral activity on clinical isolates of SARS-CoV and SARS-CoV-2 in Vero E6 cells revealed that the 50% cytopathic effect was similar for both viruses but much higher than the RNA suppression. Lower susceptibilities of SARS-CoV and SARS-CoV-2 clinical isolates to remdesivir were also measured for the Hong Kong/VM20001061/2020 strain.[37] This study also suggested that remdesivir should be considered as a combination therapy with emetine based on *in vitro* synergy.

A correlation of the *in vitro* activity of a compound with *in vivo* activity is expected but not easily achieved. Furthermore, agents with broad activity against viruses/microorganisms may act through host-derived mechanisms that are cell-specific. Identification of these mechanisms will be critical in the future repurposing of drugs in infectious diseases. *In vivo* drug concentrations are measured in blood, but drug concentrations at the site of infection must also be considered. For respiratory viral infections, the concentrations achieved in the lung parenchyma may determine the efficacy of a given drug. For example, Oseltamivir has high bioavailability and penetrates sites of infection at concentrations that are sufficient to inhibit influenza replication.[38]

The C_{max} of oral OZ277 is achieved within 1.5−5 h, and then plasma concentration declines with a mean $T_{1/2}$ of 2−4 h. Three doses were given to patients with malaria for 7 days, and the AUC was calculated from 0, 3, and 8 h concentrations on day 0 and day 6. After 7 days, mean plasma concentrations increased at all three time points.[39] The AUC was 40−239 ng*h/mL on day 0 and 79−408 ng*h/mL on day 6. The 3 h day 0 and day 6 mean plasma concentrations ranged from 8−

https://doi.org/10.1021/acsinfecdis.1c00053
ACS Infect. Dis. XXXX, XXX, XXX−XXX

40 ng/mL to 14−68 ng/mL, respectively. The reported C_{max} of OZ277 is ∼60 ng/mL,[40] which translates to an *in vitro* concentration of 0.1 μM. The AUC 3745 (last) and 1100 (48−72 h) ng*h/mL are calculated as the *in vitro* concentrations of 13 μM and 4 μM, respectively. For AS, the C_{max} after an intravenous dose is 3260 ng/mL or 3.2 mg/L,[41] calculated to an *in vitro* level of 8 μM. Pharmacokinetic data of OZ418 have only been reported in mice.[42] A single oral dose of 400 mg/kg yielded a C_{max} of 190 (185−231) μg/mL and an AUC of 9,303.8 μg/h/mL. A special feature of the OZ418 pharmacokinetic profile was its long elimination half-life of 38.7 h. This has been attributed to blood stability and slow clearance, parameters that are relevant to virus infection in tissues. Although these data are promising, there are currently no pharmacokinetic data for OZ418 in humans. Based on the calculations for OZ277, and the auxiliary role of vimentin in virus trafficking, repurposing OZ for human CoV, specifically SARS-CoV-2, might be feasible as a combination therapy. Considerations for drug combination include, but are not limited to, piperaquine, remdesivir, and apilimod.[43] A recent open label small clinical trial of oral artemisinin-piperaquine suggested that in patients with mild-to-moderate COVID-19, the time to undetectable SARS-CoV-2 RNA was significantly shorter in the treated group than in the control group (hydroxychloroquine/Arbidol).[44]

METHODS

Cell Lines, Viruses, and Compounds. Vero (Vervet monkey kidney epithelial cells, ATCC CCL-81, from Dr. Gary Hayward, Johns Hopkins University) and LLC-MK2 (Rhesus monkey kidney epithelial cells, ATCC CCL-7, from Dr. Kelly Henrickson, Medical College of Wisconsin) were cultured in DMEM (Millipore Sigma, St. Louis, MO) supplemented with 10% FBS (Corning, Oneonta, NY, USA), penicillin, streptomycin, HEPES, L-glutamine, and amphotericin B. Human foreskin fibroblasts (ATCC, CRL-2088) were cultured in DMEM supplemented with 10% FBS. Vero E6 monkey kidney cells (ATCC CRL-1586) and Calu-3 human lung adenocarcinoma cells (ATCC HTB-55) were used for infection with SARS-CoV-2. HCoV-NL63 (Zeptometrix, Franklin, MA, USA) and HCoV-OC43 (ATCC VR-1558, from Dr. Kelly Henrickson) were used for the infection of cells at a multiplicity of infection (MOI) of 0.001 unless otherwise specified. SARS-CoV-2 strain USA_WA1/2020 was used for infection of Vero E6 and Calu-3, at an MOI of 0.05. Cells were cultured in DMEM supplemented with 4% FBS postinfection with NL63 and OC43 and either 2% or 4% postinfection with SARS-CoV-2 along with varying concentrations of the compounds. Cells treated with DMSO were used as negative controls, and emetine or remdesivir (Sigma-Aldrich, St. Louis, MO, USA) was used as a positive control for CoV inhibition. The synthesis of ozonides 277 and 418 has been reported previously,[30,45,46] and their purity was determined by elemental analysis. Artesunate (AS) was purchased from Millipore Sigma.

Quantitative Real-Time Reverse-Transcription PCR (qRT-PCR) Analysis. Total cellular RNA was obtained from infected or noninfected cell cultures and isolated using the RNEasy Mini Kit (Qiagen, Germantown, MD), according to the manufacturer's instructions. Secreted viral RNA was isolated from 50 μL of cell culture supernatants using the QIAamp Viral RNA Mini Kit (Qiagen, Germantown, MD). RNA was reverse transcribed to cDNA using the RevertAid first Strand cDNA Synthesis Kit (Thermo Fisher Scientific, Waltham, MA) and quantified by real-time RT-PCR using PowerUP SYBR Green Master Mix (Thermo Fisher Scientific, Waltham, MA) following the manufacturer's instructions. All qRT-PCR assays included three sets of control wells: no reverse transcriptase, no cDNA template, or water only. The following primer pairs were used: OC43-F, 5′-GCTCAGGAAGGTCTGCTCC-3′; OC43-R, 5′-TCCTGCACTAGAGGCTCTGC-3′;[17] NL63-F, 5′-AGGACCTTAAATTCAGACAACGTTCT-3′; NL63-R, 5′-GATTACGTTTGCGATTACCAAGACT-3′;[17] GAPDH-F, 5′-TTGGTATCGTGGAAGGACTC-3′; and GAPDH-R, 5′-ACAGTCTTCTGGGTGGCAGT-3′.[47] Real-time PCR was performed on a Bio-Rad CFX Connect system (Bio-Rad, Hercules, CA).

Quantitative rRT-PCR. The CDC 2019-Novel Coronavirus (2019-nCOV) Real-Time RT-PCR Diagnostic Panel was used to measure the inhibition of SARS-CoV-2 in Calu-3 and Vero E6 cells. The primer/probe system is described below. AccuPlex SARS CoV-2 Reference Material was used to construct a standard curve. The following primer sets were used: 2019-nCoV_N1-F, 5′-GACCCCAAAATCAGCGAAAT-3′; 2019-nCoV_N1-R, 5′-TCTGGTTACTGCCAGTTGAATCTG-3′; 2019-nCoV_N1 Probe, 5′-ACCCCGCATTACGTTTGGTGGACC-3′; 2019-nCoV_N2-F, 5′-TTACAAACATTGGCCGCAAA-3′; 2019-nCoV_N2-R, 5′-GCGCGACATTCCGAAGAA-3′; and 2019-nCoV_N2 Probe, 5′-ACAATTTGCCCCCAGCGCTTCAG-3′. Relative viral RNA copies were calculated by 10^x where x represents log viral RNA copies/mL compared to infected cells.

Inhibition of SARS-CoV-2 in Vero E6 Cells. An end point titration assay for $TCID_{/50}$ PFU determinations was used for SARS-CoV-2 inhibition in Vero E6. Vero E6 monolayers in 96 well plates were infected at an MOI of 0.05 with SARS CoV-2 in DMEM + 2% FBS and incubated for 1 h at 37 °C, 5% CO_2. Inoculum was aspirated, and cells were rinsed once with DMEM (100 μL) without FBS. Serial 2-fold dilutions of compounds in DMEM 2% FBS were added to duplicate wells and incubated for 72 h at 37 °C, 5% CO_2. Monolayers were stained with 2% crystal violet in a 20% methanol solution.

Toxicity Assays. A 3-(4,5-dimethyl-2-thiazolyl)-2,5-diphenyl-2H-tetrazolium bromide (MTT) assay was performed according to the manufacturer's instructions (Millipore Sigma). Noninfected cells were treated with OZ418, OZ277, or AS for 72 h and 20 μL/well of MTT ([3-(4,5-dimethyl-2-thiazolyl)-2,5-diphenyl-2H-tetrazolium bromide], and 5 mg/mL in phosphate-buffered saline (PBS) was added to each well. After shaking at 150 rpm for 5 min, the plates were incubated at 37 °C for 2−3 h. Conversion of the yellow solution to dark blue formazan by mitochondrial dehydrogenases of living cells was quantified by measuring absorbance at 560 nm. Toxicity of OZ418 in HFFs has been previously reported.[30]

Western Blot. Two × 10^6 HFFs were plated in 6 well plates, and the following day the cells were infected with OC43 (MOI = 1) for 1 h. Cells were then washed with PBS once, and OZ418 (30 μM), OZ277 (15 μM), AS (30 μM), emetine (200 nM), or DMSO was added to infected cells. All drugs were diluted in DMEM containing 4% FBS along with noninfected and infected nontreated (DMSO only) controls. At 72 h postinfection, the cells were washed with PBS and lysed in cell lysis buffer (Promega) containing protease (Roche) and phosphatase (Thermo Scientific) inhibitors. Lysate from each condition (50 μg) was separated on 10% SDS-PAGE for

https://doi.org/10.1021/acsinfecdis.1c00053
ACS Infect. Dis. XXXX, XXX, XXX−XXX

detection of the OC43 antigen, and 25 μg of lysate from each condition was analyzed for β-actin (Sigma, 1:10,000) as the loading control. Anti-coronavirus monoclonal antibody, OC-43 strain, clone 541-8F (Merck Millipore, MAB9012) (1:250) was used to detect the OC43 antigen (not defined).

Combination. The combination of OZ418 and RDV against OC43 was measured by Western blot. Two × 10^6 HFFs were seeded in 6 well plates, and 2 wells were used for each condition. Cells were infected with OC43 (MOI = 1) for 1 h, washed, and then treated with various concentrations of OZ418 and RDV and their respective combinations for 72 h. Cells were lysed using lysis buffer containing protease inhibitors, and 25 μg of the lysate was analyzed by Western blot for detection of the OC43 antigen as mentioned earlier. The combination effect was tested in SARS-CoV-2-infected Calu-3 and Vero E6 based on the biomass determination in 12 well plates. Staining of the cell monolayers with 2% crystal violet in a 20% methanol solution was followed by solubilization in 10% acetic acid followed by OD determination at 595 nm. The relative biomass was calculated compared to noninfected cells and is represented as %.

Statistical Analysis. Dose−response curves were generated as described previously.[48] The EC_{50} and CC_{50} values were calculated using GraphPad Prism software using the nonlinear curve fitting and the exponential form of the median effect equation, where percent inhibition = $1/[1+ (CC_{50}$ or $EC_{50}/$ drug concentration)$m]$, where m is a parameter that reflects the slope of the concentration−response curve.

CONCLUSION

OZ418 is an inhibitor of SARS-COV-2 *in vitro* as well as the less pathogenic α- and β-CoV. It may be considered for further drug combination studies with other agents.

ASSOCIATED CONTENT

Supporting Information

The Supporting Information is available free of charge at https://pubs.acs.org/doi/10.1021/acsinfecdis.1c00053.

Figure S1, anti SARS-CoV-2 activity of OZ439 in Vero and Calu-3 cells; Figure S2, effect of combination of OZ418 and remdesivir on SARS-CoV-2-infected Calu-3 cells (PDF)

AUTHOR INFORMATION

Corresponding Author

Ravit Arav-Boger − *Department of Pediatrics, Division of Infectious Disease, Medical College of Wisconsin, Milwaukee, Wisconsin 53226, United States;* orcid.org/0000-0002-5363-167X; Phone: 414 337 7070; Email: rboger@mcw.edu; Fax: 414 337 7093

Authors

Ayan Kumar Ghosh − *Department of Pediatrics, Division of Infectious Disease, Medical College of Wisconsin, Milwaukee, Wisconsin 53226, United States*

Halli Miller − *Department of Pediatrics, Division of Infectious Disease, Medical College of Wisconsin, Milwaukee, Wisconsin 53226, United States*

Konstance Knox − *Coppe Healthcare Solutions, Waukesha, Wisconsin 53186, United States*

Madhuchhanda Kundu − *Coppe Healthcare Solutions, Waukesha, Wisconsin 53186, United States*

Kelly J. Henrickson − *Department of Pediatrics, Division of Infectious Disease, Medical College of Wisconsin, Milwaukee, Wisconsin 53226, United States*

Complete contact information is available at: https://pubs.acs.org/10.1021/acsinfecdis.1c00053

Author Contributions

#A.K.G. and H.M. contributed equally to this work.

Notes

The authors declare no competing financial interest.

ACKNOWLEDGMENTS

We thank Natalie Thornburg, Ph.D., CDC Principal Investigator, and the UTMB World Reference Center for Emerging Viruses and Arboviruses (WRCEVA) for providing SARS-CoV-2 strain USA_WA1/2020. We thank Jonathan Vennerstrom, Department of Pharmaceutical Sciences, University of Nebraska Medical Center, for providing the ozonides (OZ277, OZ418, and OZ439) for the study.

REFERENCES

(1) Zhou, P., Yang, X. L., Wang, X. G., Hu, B., Zhang, L., Zhang, W., Si, H. R., Zhu, Y., Li, B., Huang, C. L., Chen, H. D., Chen, J., Luo, Y., Guo, H., Jiang, R. D., Liu, M. Q., Chen, Y., Shen, X. R., Wang, X., Zheng, X. S., Zhao, K., Chen, Q. J., Deng, F., Liu, L. L., Yan, B., Zhan, F. X., Wang, Y. Y., Xiao, G. F., and Shi, Z. L. (2020) A pneumonia outbreak associated with a new coronavirus of probable bat origin. *Nature 579*, 270−273.

(2) Dhama, K., Sharun, K., Tiwari, R., Dadar, M., Malik, Y. S., Singh, K. P., and Chaicumpa, W. (2020) COVID-19, an emerging coronavirus infection: advances and prospects in designing and developing vaccines, immunotherapeutics, and therapeutics. *Hum. Vaccines Immunother. 16*, 1232−1238.

(3) Beigel, J. H., Tomashek, K. M., Dodd, L. E., Mehta, A. K., Zingman, B. S., Kalil, A. C., Hohmann, E., Chu, H. Y., Luetkemeyer, A., Kline, S., Lopez de Castilla, D., Finberg, R. W., Dierberg, K., Tapson, V., Hsieh, L., Patterson, T. F., Paredes, R., Sweeney, D. A., Short, W. R., Touloumi, G., Lye, D. C., Ohmagari, N., Oh, M. D., Ruiz-Palacios, G. M., Benfield, T., Fatkenheuer, G., Kortepeter, M. G., Atmar, R. L., Creech, C. B., Lundgren, J., Babiker, A. G., Pett, S., Neaton, J. D., Burgess, T. H., Bonnett, T., Green, M., Makowski, M., Osinusi, A., Nayak, S., Lane, H. C., and Members, A.-S. G. (2020) Remdesivir for the Treatment of Covid-19 - Final Report. *N. Engl. J. Med. 383*, 1813−1826.

(4) Pyrc, K., Berkhout, B., and van der Hoek, L. (2007) Identification of new human coronaviruses. *Expert Rev. Anti-Infect. Ther. 5*, 245−253.

(5) Chu, C. M., Cheng, V. C., Hung, I. F., Wong, M. M., Chan, K. H., Chan, K. S., Kao, R. Y., Poon, L. L., Wong, C. L., Guan, Y., Peiris, J. S., Yuen, K. Y., and Group, H. U. S. S. (2004) Role of lopinavir/ritonavir in the treatment of SARS: initial virological and clinical findings. *Thorax 59*, 252−256.

(6) Cao, B., Wang, Y., Wen, D., Liu, W., Wang, J., Fan, G., Ruan, L., Song, B., Cai, Y., Wei, M., Li, X., Xia, J., Chen, N., Xiang, J., Yu, T., Bai, T., Xie, X., Zhang, L., Li, C., Yuan, Y., Chen, H., Li, H., Huang, H., Tu, S., Gong, F., Liu, Y., Wei, Y., Dong, C., Zhou, F., Gu, X., Xu, J., Liu, Z., Zhang, Y., Li, H., Shang, L., Wang, K., Li, K., Zhou, X., Dong, X., Qu, Z., Lu, S., Hu, X., Ruan, S., Luo, S., Wu, J., Peng, L., Cheng, F., Pan, L., Zou, J., Jia, C., Wang, J., Liu, X., Wang, S., Wu, X., Ge, Q., He, J., Zhan, H., Qiu, F., Guo, L., Huang, C., Jaki, T., Hayden, F. G., Horby, P. W., Zhang, D., and Wang, C. (2020) A Trial of Lopinavir-Ritonavir in Adults Hospitalized with Severe Covid-19. *N. Engl. J. Med. 382*, 1787−1799.

(7) Ferner, R. E., and Aronson, J. K. (2020) Chloroquine and hydroxychloroquine in covid-19. *BMJ. 369*, m1432.

(8) Ferner, R. E., and Aronson, J. K. (2020) Remdesivir in covid-19. *BMJ. 369*, m1610.
(9) Luo, P., Liu, Y., Qiu, L., Liu, X., Liu, D., and Li, J. (2020) Tocilizumab treatment in COVID-19: A single center experience. *J. Med. Virol. 92*, 814−818.
(10) Chen, P., Nirula, A., Heller, B., Gottlieb, R. L., Boscia, J., Morris, J., Huhn, G., Cardona, J., Mocherla, B., Stosor, V., Shawa, I., Adams, A. C., Van Naarden, J., Custer, K. L., Shen, L., Durante, M., Oakley, G., Schade, A. E., Sabo, J., Patel, D. R., Klekotka, P., and Skovronsky, D. M. (2021) Investigators, B.-. SARS-CoV-2 Neutralizing Antibody LY-CoV555 in Outpatients with Covid-19. *N. Engl. J. Med. 384*, 229−237.
(11) Efferth, T. (2018) Beyond malaria: The inhibition of viruses by artemisinin-type compounds. *Biotechnol. Adv. 36*, 1730−1737.
(12) Charman, S. A., Arbe-Barnes, S., Bathurst, I. C., Brun, R., Campbell, M., Charman, W. N., Chiu, F. C., Chollet, J., Craft, J. C., Creek, D. J., Dong, Y., Matile, H., Maurer, M., Morizzi, J., Nguyen, T., Papastogiannidis, P., Scheurer, C., Shackleford, D. M., Sriraghavan, K., Stingelin, L., Tang, Y., Urwyler, H., Wang, X., White, K. L., Wittlin, S., Zhou, L., and Vennerstrom, J. L. (2011) Synthetic ozonide drug candidate OZ439 offers new hope for a single-dose cure of uncomplicated malaria. *Proc. Natl. Acad. Sci. U. S. A. 108*, 4400−4405.
(13) Xue, J., Wang, X., Dong, Y., Vennerstrom, J. L., and Xiao, S. H. (2014) Effect of ozonide OZ418 against Schistosoma japonicum harbored in mice. *Parasitol. Res. 113*, 3259−3266.
(14) Patil, C., Katare, S., Baig, M., and Doifode, S. (2014) Fixed dose combination of arterolane and piperaquine: a newer prospect in antimalarial therapy. *Ann. Med. Health Sci. Res. 4*, 466−471.
(15) Phyo, A. P., Jittamala, P., Nosten, F. H., Pukrittayakamee, S., Imwong, M., White, N. J., Duparc, S., Macintyre, F., Baker, M., and Mohrle, J. J. (2016) Antimalarial activity of artefenomel (OZ439), a novel synthetic antimalarial endoperoxide, in patients with Plasmodium falciparum and Plasmodium vivax malaria: an open-label phase 2 trial. *Lancet Infect. Dis. 16*, 61−69.
(16) Dong, Y., Wang, X., Kamaraj, S., Bulbule, V. J., Chiu, F. C., Chollet, J., Dhanasekaran, M., Hein, C. D., Papastogiannidis, P., Morizzi, J., Shackleford, D. M., Barker, H., Ryan, E., Scheurer, C., Tang, Y., Zhao, Q., Zhou, L., White, K. L., Urwyler, H., Charman, W. N., Matile, H., Wittlin, S., Charman, S. A., and Vennerstrom, J. L. (2017) Structure-Activity Relationship of the Antimalarial Ozonide Artefenomel (OZ439). *J. Med. Chem. 60*, 2654−2668.
(17) Shen, L., Niu, J., Wang, C., Huang, B., Wang, W., Zhu, N., Deng, Y., Wang, H., Ye, F., Cen, S., and Tan, W. (2019) High-Throughput Screening and Identification of Potent Broad-Spectrum Inhibitors of Coronaviruses. *J. Virol 93*, e00023-19.
(18) Roy, S., Kapoor, A., Zhu, F., Mukhopadhyay, R., Ghosh, A. K., Lee, H., Mazzone, J., Posner, G. H., and Arav-Boger, R. (2020) Artemisinins target the intermediate filament protein vimentin for human cytomegalovirus inhibition. *J. Biol. Chem. 295*, 15013−15028.
(19) Yu, Y. T., Chien, S. C., Chen, I. Y., Lai, C. T., Tsay, Y. G., Chang, S. C., and Chang, M. F. (2016) Surface vimentin is critical for the cell entry of SARS-CoV. *J. Biomed. Sci. 23*, 14.
(20) Adjuik, M., Babiker, A., Garner, P., Olliaro, P., Taylor, W., and White, N. (2004) Artesunate combinations for treatment of malaria: meta-analysis. *Lancet 363*, 9−17.
(21) Jones, K. L., Donegan, S., and Lalloo, D. G. (2007) Artesunate versus quinine for treating severe malaria. *Cochrane. Database. Syst. Rev. 2012*, CD005967.
(22) Efferth, T., Marschall, M., Wang, X., Huong, S. M., Hauber, I., Olbrich, A., Kronschnabl, M., Stamminger, T., and Huang, E. S. (2002) Antiviral activity of artesunate towards wild-type, recombinant, and ganciclovir-resistant human cytomegaloviruses. *J. Mol. Med. (Heidelberg, Ger.) 80*, 233−242.
(23) Efferth, T., Romero, M. R., Wolf, D. G., Stamminger, T., Marin, J. J., and Marschall, M. (2008) The antiviral activities of artemisinin and artesunate. *Clin. Infect. Dis. 47*, 804−811.
(24) Oiknine-Djian, E., Weisblum, Y., Panet, A., Wong, H. N., Haynes, R. K., and Wolf, D. G. (2018) The Artemisinin Derivative Artemisone Is a Potent Inhibitor of Human Cytomegalovirus Replication. *Antimicrob. Agents Chemother. 62*, e00288-18.
(25) He, R., Mott, B. T., Rosenthal, A. S., Genna, D. T., Posner, G. H., and Arav-Boger, R. (2011) An artemisinin-derived dimer has highly potent anti-cytomegalovirus (CMV) and anti-cancer activities. *PLoS One 6*, e24334.
(26) O'Neill, P. M., Barton, V. E., and Ward, S. A. (2010) The molecular mechanism of action of artemisinin−the debate continues. *Molecules 15*, 1705−1721.
(27) Paeshuyse, J., Coelmont, L., Vliegen, I., Van hemel, J., Vandenkerckhove, J., Peys, E., Sas, B., De Clercq, E., and Neyts, J. (2006) Hemin potentiates the anti-hepatitis C virus activity of the antimalarial drug artemisinin. *Biochem. Biophys. Res. Commun. 348*, 139−144.
(28) Efferth, T., Marschall, M., Wang, X., Huong, S. M., Hauber, I., Olbrich, A., Kronschnabl, M., Stamminger, T., and Huang, E. S. (2002) Antiviral activity of artesunate towards wild-type, recombinant, and ganciclovir-resistant human cytomegaloviruses. *J. Mol. Med. 80*, 233−242.
(29) Cao, R., Hu, H., Li, Y., Wang, X., Xu, M., Liu, J., Zhang, H., Yan, Y., Zhao, L., Li, W., Zhang, T., Xiao, D., Guo, X., Li, Y., Yang, J., Hu, Z., Wang, M., and Zhong, W. (2020) Anti-SARS-CoV-2 Potential of Artemisinins In Vitro. *ACS Infect. Dis. 6*, 2524−2531.
(30) Wang, Y., Mukhopadhyay, R., Roy, S., Kapoor, A., Su, Y. P., Charman, S. A., Chen, G., Wu, J., Wang, X., Vennerstrom, J. L., and Arav-Boger, R. (2019) Inhibition of Cytomegalovirus Replication with Extended-Half-Life Synthetic Ozonides. *Antimicrob. Agents Chemother. 63*, e01735-18.
(31) Kim, J., Yang, C., Kim, E. J., Jang, J., Kim, S. J., Kang, S. M., Kim, M. G., Jung, H., Park, D., and Kim, C. (2016) Vimentin filaments regulate integrin-ligand interactions by binding to the cytoplasmic tail of integrin beta3. *J. Cell Sci. 129*, 2030−2042.
(32) Kreis, S., Schonfeld, H. J., Melchior, C., Steiner, B., and Kieffer, N. (2005) The intermediate filament protein vimentin binds specifically to a recombinant integrin alpha2/beta1 cytoplasmic tail complex and co-localizes with native alpha2/beta1 in endothelial cell focal adhesions. *Exp. Cell Res. 305*, 110−121.
(33) Efferth, T. (2006) Molecular pharmacology and pharmacogenomics of artemisinin and its derivatives in cancer cells. *Curr. Drug Targets 7*, 407−421.
(34) Buckley, S. T., Medina, C., and Ehrhardt, C. (2010) Differential susceptibility to epithelial-mesenchymal transition (EMT) of alveolar, bronchial and intestinal epithelial cells in vitro and the effect of angiotensin II receptor inhibition. *Cell Tissue Res. 342*, 39−51.
(35) Li, Z., Paulin, D., Lacolley, P., Coletti, D., and Agbulut, O. (2020) Vimentin as a target for the treatment of COVID-19. *BMJ. Open Respir Res. 7*, e000623.
(36) Malin, J. J., Suarez, I., Priesner, V., Fatkenheuer, G., and Rybniker, J. (2020) Remdesivir against COVID-19 and Other Viral Diseases. *Clin. Microbiol. Rev. 34*, e00162-20.
(37) Choy, K. T., Wong, A. Y., Kaewpreedee, P., Sia, S. F., Chen, D., Hui, K. P. Y., Chu, D. K. W., Chan, M. C. W., Cheung, P. P., Huang, X., Peiris, M., and Yen, H. L. (2020) Remdesivir, lopinavir, emetine, and homoharringtonine inhibit SARS-CoV-2 replication in vitro. *Antiviral Res. 178*, 104786.
(38) Davies, B. E. (2010) Pharmacokinetics of oseltamivir: an oral antiviral for the treatment and prophylaxis of influenza in diverse populations. *J. Antimicrob. Chemother. 65* (2), ii5−ii10.
(39) Gautam, A., Ahmed, T., Sharma, P., Varshney, B., Kothari, M., Saha, N., Roy, A., Moehrle, J. J., and Paliwal, J. (2011) Pharmacokinetics and pharmacodynamics of arterolane maleate following multiple oral doses in adult patients with P. falciparum malaria. *J. Clin. Pharmacol. 51*, 1519−1528.
(40) Valecha, N., Savargaonkar, D., Srivastava, B., Rao, B. H., Tripathi, S. K., Gogtay, N., Kochar, S. K., Kumar, N. B., Rajadhyaksha, G. C., Lakhani, J. D., Solanki, B. B., Jalali, R. K., Arora, S., Roy, A., Saha, N., Iyer, S. S., Sharma, P., and Anvikar, A. R. (2016) Comparison of the safety and efficacy of fixed-dose combination of arterolane maleate and piperaquine phosphate with chloroquine in

https://doi.org/10.1021/acsinfecdis.1c00053
ACS Infect. Dis. XXXX, XXX, XXX−XXX

acute, uncomplicated Plasmodium vivax malaria: a phase III, multicentric, open-label study. *Malar. J. 15*, 42.
(41) Byakika-Kibwika, P., Lamorde, M., Mayito, J., Nabukeera, L., Mayanja-Kizza, H., Katabira, E., Hanpithakpong, W., Obua, C., Pakker, N., Lindegardh, N., Tarning, J., de Vries, P. J., and Merry, C. (2012) Pharmacokinetics and pharmacodynamics of intravenous artesunate during severe malaria treatment in Ugandan adults. *Malar. J. 11*, 132.
(42) Leonidova, A., Vargas, M., Huwyler, J., and Keiser, J. (2016) Pharmacokinetics of the Antischistosomal Lead Ozonide OZ418 in Uninfected Mice Determined by Liquid Chromatography-Tandem Mass Spectrometry. *Antimicrob. Agents Chemother. 60*, 7364−7371.
(43) Kang, Y. L., Chou, Y. Y., Rothlauf, P. W., Liu, Z., Soh, T. K., Cureton, D., Case, J. B., Chen, R. E., Diamond, M. S., Whelan, S. P. J., and Kirchhausen, T. (2020) Inhibition of PIKfyve kinase prevents infection by Zaire ebolavirus and SARS-CoV-2. *Proc. Natl. Acad. Sci. U. S. A. 117*, 20803−20813.
(44) Li, G., Yuan, M., Li, H., Deng, C., Wang, Q., Tang, Y., Zhang, H., Yu, W., Xu, Q., Zou, Y., Yuan, Y., Guo, J., Jin, C., Guan, X., Xie, F., and Song, J. (2021) Safety and efficacy of artemisinin-piperaquine for treatment of COVID-19: an open-label, non-randomised and controlled trial. *Int. J. Antimicrob. Agents 57*, 106216.
(45) Fugi, M. A., Wittlin, S., Dong, Y., and Vennerstrom, J. L. (2010) Probing the antimalarial mechanism of artemisinin and OZ277 (arterolane) with nonperoxidic isosteres and nitroxyl radicals. *Antimicrob. Agents Chemother. 54*, 1042−1046.
(46) Vennerstrom, J. L., Arbe-Barnes, S., Brun, R., Charman, S. A., Chiu, F. C., Chollet, J., Dong, Y., Dorn, A., Hunziker, D., Matile, H., McIntosh, K., Padmanilayam, M., Santo Tomas, J., Scheurer, C., Scorneaux, B., Tang, Y., Urwyler, H., Wittlin, S., and Charman, W. N. (2004) Identification of an antimalarial synthetic trioxolane drug development candidate. *Nature 430*, 900−904.
(47) Fan, Y. H., Roy, S., Mukhopadhyay, R., Kapoor, A., Duggal, P., Wojcik, G. L., Pass, R. F., and Arav-Boger, R. (2016) Role of nucleotide-binding oligomerization domain 1 (NOD1) and its variants in human cytomegalovirus control in vitro and in vivo. *Proc. Natl. Acad. Sci. U. S. A. 113*, E7818−E7827.
(48) Cai, H., Kapoor, A., He, R., Venkatadri, R., Forman, M., Posner, G. H., and Arav-Boger, R. (2014) In vitro combination of anti-cytomegalovirus compounds acting through different targets: role of the slope parameter and insights into mechanisms of Action. *Antimicrob. Agents Chemother. 58*, 986−994.

https://doi.org/10.1021/acsinfecdis.1c00053
ACS Infect. Dis. XXXX, XXX, XXX−XXX